

## Rotational and Vibrational Transitions in Molecular Collisions

*J. Peter Toennies*

Max-Planck-Institut für Strömungsforschung, Böttingerstr. 6–8,  
D-3400 Göttingen, Federal Republic of Germany.

### *Abstract*

Recent progress in understanding collision processes involving rotational and vibrational excitation in collisions of atoms (ions) with molecules in terms of simple models is illustrated for two systems. Rotational excitation of N<sub>2</sub> in collision with He at 27 meV can be explained by an optical model. A more quantitative agreement is achieved by cross sections calculated exactly for the model potential of Tang and Toennies. Vibrational excitation probabilities for resolved single mode excitation of CF<sub>4</sub> in small angle 10 eV ion collisions follow a Poisson distribution indicating a breathing sphere forced oscillator behaviour. The results are in good agreement with classical calculations based on infrared coupling constants. At large angles in Na<sup>+</sup>-CF<sub>4</sub> collisions the first evidence for a direct impulsive interaction of the ions with the F atoms is presented.

### 1. Introduction

In the region of thermal energies ( $10^{-2}$ –5 eV) molecular collisions generally involve rotational transitions and, if the energies are high enough, vibrational transitions as well. Thus these two processes are fundamental for an understanding of gas kinetic processes, such as transport coefficients, relaxation rates in shock waves and nozzle flow, as well as for an understanding of energy transfer in chemical lasers, chemically reactive systems and even in outer space where collisions excite molecules into states which emit microwaves observable on Earth.

From a more basic point of view these processes are of interest for essentially two reasons: (1) They provide the most direct insight into the van der Waals potential. Thus from a best fit of scattering cross sections it is possible to obtain highly accurate potential hypersurfaces. (2) As the simplest of all the possible inelastic collision processes they serve as a testing ground for scattering theories, which can then be applied to more complex problems such as reactive scattering.

Beam scattering studies have now been successfully carried out on a large number of systems. Much of the recent work has been reviewed previously (Toennies 1976; Faubel and Toennies 1977). The most carefully studied systems with state resolved excitation both from the theoretical and experimental point of view are alkali-halide rare gases (Meyer and Toennies 1981, 1982), Li<sup>+</sup>-H<sub>2</sub> (Faubel and Toennies 1979), H<sup>+</sup>-H<sub>2</sub> (Rudolph and Toennies 1976; Schmidt *et al.* 1976), He/Ne-H<sub>2</sub> (Gentry and Giese 1977; Buck *et al.* 1978), H<sub>2</sub>-H<sub>2</sub> (Buck *et al.* 1981), and more recently Na<sub>2</sub>-rare gases (Bergmann *et al.* 1979, 1981), and as discussed here He-N<sub>2</sub> and CH<sub>4</sub> (Faubel *et al.* 1980), O<sub>2</sub> (Faubel *et al.* 1982) and CO (Kohl *et al.* 1982). State resolved vibrational excitation in neutral systems has only been seen in K-N<sub>2</sub>

(Ross *et al.* 1981), although work is in progress on  $\text{CF}_4$  and  $\text{SF}_6$  in collision with Ne and Ar at  $E_{\text{cm}} = 1$  eV (Eccles *et al.* 1982). Alkali-ion-molecule systems (Faubel and Toennies 1977) have been more extensively studied and vibrational excitation in systems such as  $\text{Li}^+-\text{H}_2$  and  $\text{N}_2$  are expected to closely mimic neutral systems. Other systems such as  $\text{H}^+-\text{H}_2$  (Rudolph and Toennies 1976),  $\text{H}^+-\text{CO}_2$  (Krutein and Linder 1977; Bischof *et al.* 1981; Gierz *et al.* 1982a) and  $\text{H}^+-\text{O}_2$  (Gianturco *et al.* 1980) reveal significant effects of chemical interactions, while the systems  $\text{Li}^+-\text{CO}_2$  and  $\text{N}_2\text{O}$  (Faubel and Toennies 1977),  $\text{Li}^+(\text{H}^+)-\text{CF}_4$  and  $\text{SF}_6$  (Ellenbroek *et al.* 1980, 1982), and  $\text{H}^+$  fluorinated hydrocarbons (Noll 1982) can be explained by strong electrostatic interactions.

In the present paper we survey briefly some of the recent results in these areas coming from our laboratory. The recent emphasis of our work has been to develop models to increase our physical insight into the basic laws underlying the scattering potential and the dynamics. This is illustrated for rotational excitation in  $\text{He}-\text{N}_2$  and for vibrational excitation of  $\text{CF}_4$  in collisions with  $\text{H}^+$  and  $\text{Na}^+$  ions.

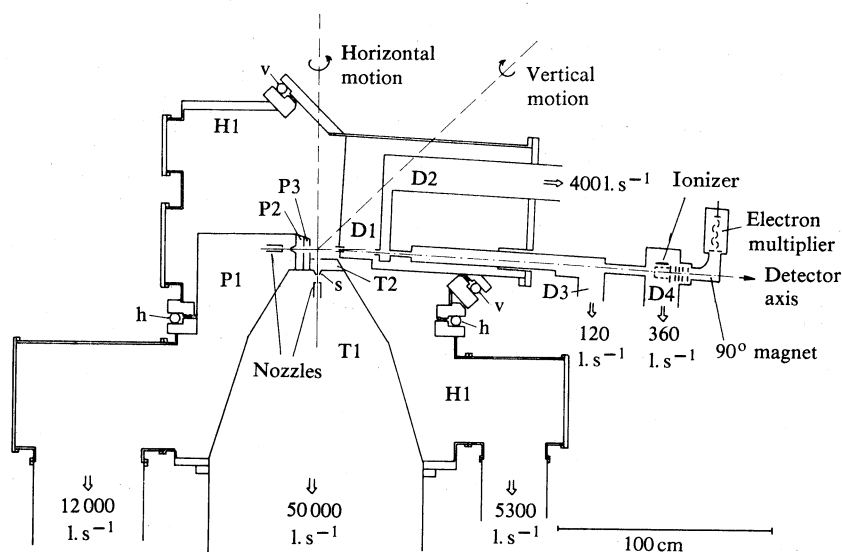


**Fig. 1.** Schematic diagram of the crossed supersonic molecular beam TOF apparatus. Six differential pumping stages (H1, T1, T2, P1, P2, P3) are used in the production of two well defined supersonic beams. A helium partial pressure of  $10^{-16}$  Torr in the mass spectrometer detector is maintained by four additional differential vacuum stages (D1–D4). Horizontal and vertical scattering angles are selected by motion of the ball bearing supported flanges *v* and *h*. The skimmer is marked by *s*. The flight path of 165 cm allows 1% velocity resolution.

## 2. Rotational Excitation in $\text{He}-\text{N}_2$

### (a) Apparatus

The apparatus is shown to scale in the side view drawing in Fig. 1. Two nearly monochromatic molecular beams, namely the He primary and the  $\text{N}_2$  target beam, are formed in nozzle expansions. The He beam is expanded from 200 atm (1 atm  $\equiv$  101.325 kPa) at 88 K through a  $20 \mu\text{m}$  hole and has a relative velocity spread of only 0.7% (Toennies and Winkelmann 1977; Brusdeylins *et al.* 1977). The  $\text{N}_2$  beam has a velocity spread of about 5%. The rotational temperature in the

expanded  $N_2$  beam is of the order of 6 K, and the measured rotational state populations are  $j = 0$ , 52%;  $j = 1$ , 33%; and  $j = 2$ , 15% (Faubel and Weiner 1981). After collimation by skimmers and additional differentially pumped collimators the two beams intersect in the centre of the apparatus. Scattered He atoms are observed by the mass spectrometer detector on the right-hand side of Fig. 1. The scattering angle is changed by rotating the upper part of the machine containing the detector assembly with respect to the vertical axis indicated. For observing individual rotational transitions at a given scattering angle the flight time and thus the energy change of scattered molecules is measured. For this purpose a chopper wheel 12 cm in diameter with four slots 1 mm wide is rotated through the He beam at 24 000 r.p.m. The count rate of scattered particles arriving at the detector is then recorded as a function of the time delay from the passage of a chopper slit through the He beam.

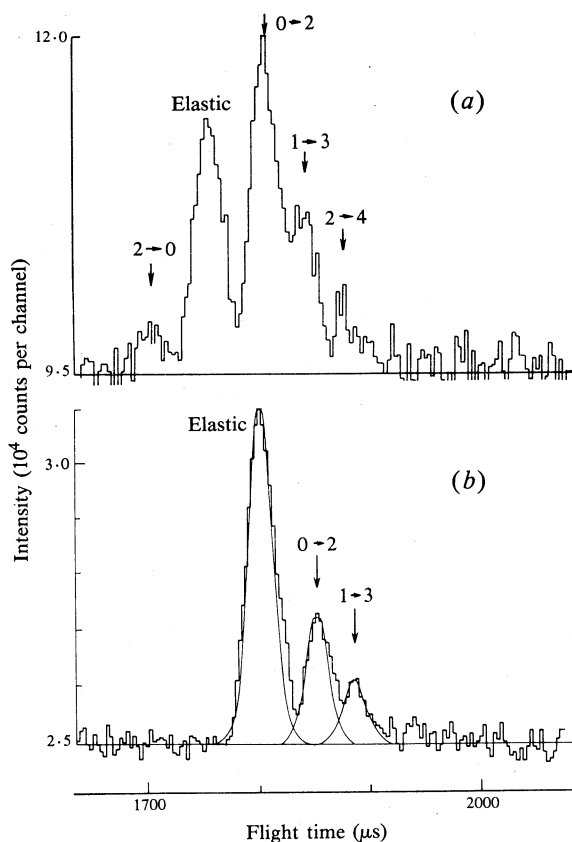


**Fig. 2.** Two typical TOF spectra of He scattered from  $N_2$ : (a)  $\theta_{lab} = 20^\circ$  and (b)  $\theta_{lab} = 39.5^\circ$ . The spectra were accumulated in a measuring time of about 14 hours. For the collision energy of  $E_{cm} = 27.7$  meV and scattering angle  $\theta_{lab} = 20^\circ$  (equivalent to  $\theta_{cm} \approx 17.5^\circ$ ), the flight time of elastically scattered He is  $1750 \mu s$ . Well separated from the elastic peak, helium which has excited the  $j_i = 0$  to  $j' = 2$  rotational transition of  $N_2$  and lost an energy of  $1.5$  meV ( $12 \text{ cm}^{-1}$ ) arrives after a flight time of  $1800 \mu s$ . The additional inelastic peaks indicated from the  $1 \rightarrow 3$ ,  $2 \rightarrow 0$  and  $2 \rightarrow 4$  rotational transitions are also observed.

Two typical time-of-flight (TOF) spectra are shown in Fig. 2. The time resolution and thus the energy level resolution are somewhat limited by apparatus effects, such as the finite chopper opening time of  $7 \mu\text{s}$  and the ratio of the ionizer length ( $\approx 1.5 \text{ cm}$ ) to the length of the total flight path (165 cm), and thus allow a velocity resolution of 1% corresponding to an energy resolution of  $0.6 \text{ meV}$  at a He energy of  $30 \text{ meV}$ . A second and more serious kinematical limitation on the energy resolution (Faubel and Toennies 1977) results from the finite velocity spreads and angular divergences of the colliding beams.

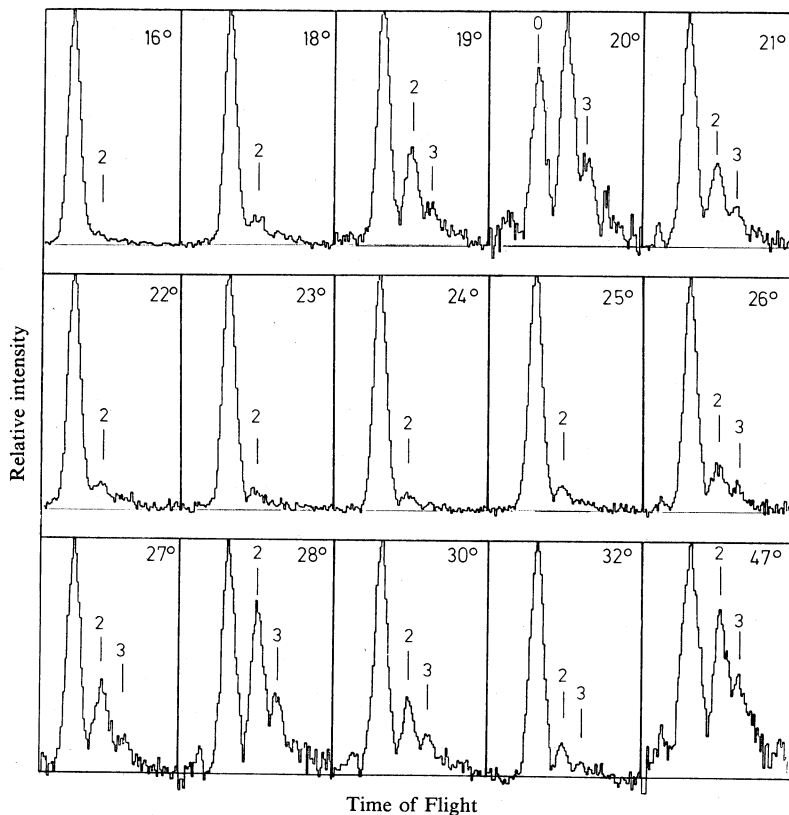


**Fig. 3.** TOF spectra measured at  $E_{\text{cm}} = 27.3 \text{ meV}$  and at various lab scattering angles. The numbers 0, 2 and 3 refer to the expected locations of the elastic and the  $j = 0 \rightarrow 2$  and  $1 \rightarrow 3$  transitions respectively. The amplitude of the largest peak has been normalized to unity. Note that at  $20^\circ$ ,  $28^\circ$  and  $47^\circ$  the inelastic peaks are especially large.

The narrow beam collimation and the long flight path lead to a drastic loss in scattering intensity. Therefore, the He partial pressure in the detector has to be lowered to less than the signal density of  $10^{-16} \text{ Torr}$  ( $= 0.133 \times 10^{-16} \text{ kPa}$ ). As shown in Fig. 1, the detector vacuum is maintained against the main chamber pressure of  $10^{-6} \text{ Torr}$  by four differential pumping stages ( $D_1$ – $D_4$ ) along the flight path. With an estimated He detection efficiency of  $10^{-5}$  the average detector count rate was about  $10 \text{ counts s}^{-1}$  and measuring times of typically 10 to 30 hours were required to obtain the TOF spectra shown in Fig. 2.

(b) TOF Spectra for He-N<sub>2</sub>

In Fig. 2 the TOF spectra measured at  $E_{\text{cm}} = 27.7$  meV clearly reveal that all the rotational transitions including the  $j = 0 \rightarrow 2$  transition ( $\Delta E = 1.5$  meV) are well resolved. In Fig. 2a, the half-width of the elastic peak at  $\theta = 20^\circ$  is about  $800 \mu\text{eV}$ . The small deexcitation peak at  $\theta_{\text{lab}} = 20^\circ$  confirms the nearly perfect relaxation of the rotational states in the N<sub>2</sub> beam.

The variation of TOF spectra is shown in Fig. 3 for a number of lab scattering angles in the range  $16^\circ$ – $47^\circ$ . At most angles the  $0 \rightarrow 2$  and  $1 \rightarrow 3$  rotational transition probabilities (indicated by 2 and 3 respectively) are quite small, being of the order of 10–20%. However, at certain specific angles  $\theta_{\text{lab}} = 20^\circ$ ,  $28^\circ$  and  $47^\circ$ , and at larger angles, the inelastic transition probabilities are comparable with the elastic probabilities.

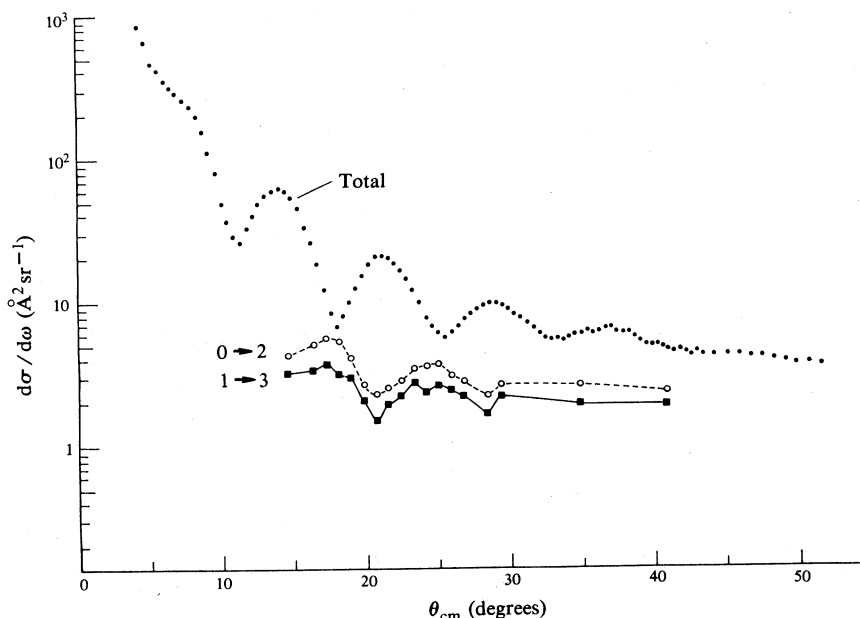


Fig. 4. Experimental c.m. total and the  $0 \rightarrow 2$  and  $1 \rightarrow 3$  rotationally inelastic cross sections for He-N<sub>2</sub> at  $E_{\text{cm}} = 27.3$  meV.

Using the measured N<sub>2</sub> initial rotational state populations the TOF spectra were corrected to yield state-to-state differential lab cross sections. These were then transformed into the c.m. system and are shown in Fig. 4 as the total and the  $0 \rightarrow 2$  and  $1 \rightarrow 3$  rotationally inelastic differential cross sections. The systematic average error in the absolute calibration (in  $\text{\AA}^2 \text{sr}^{-1}$ ) is estimated to be 5%. The accuracy of the scattering angles is  $0.2^\circ$ . Individual points have statistical errors of about 10% for cross sections less than  $5 \text{\AA}^2 \text{sr}^{-1}$  and 3% for larger cross sections.

All cross sections show well resolved Fraunhofer diffraction oscillations but, as an indication of the very shallow well of the He-N<sub>2</sub> potential, no characteristic rainbow structure is present\*. The absolute amplitude of the oscillations in the

\* Note that the presence of a potential well does lead to an additional undulation in the diffraction pattern seen in Fig. 4 at  $\theta \approx 5^\circ$ .

rotationally inelastic  $0 \rightarrow 2$  and  $1 \rightarrow 3$  transitions is slightly quenched compared with the total differential cross section. The  $1 \rightarrow 3$  differential cross section is smaller than the  $0 \rightarrow 2$  cross section, and its oscillatory structure is almost proportional to the  $0 \rightarrow 2$  cross section, with a proportionality ratio of about 0.7. This agrees remarkably well with the predictions of the infinite order sudden (IOS) factorization rule (Goldflam *et al.* 1977).

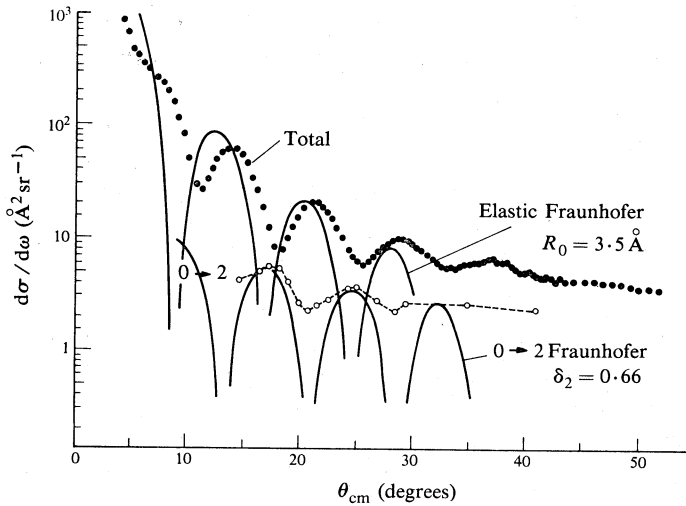


Fig. 5. Comparison for He-N<sub>2</sub> ( $E_{cm} = 27.3$  meV) of the angular distributions predicted by the Fraunhofer model with the measured distributions. The inelastic model diffraction peaks were fitted for a deformation parameter of  $\delta_2 = 0.66$  Å.

### (c) Inelastic Fraunhofer Model

Rather surprising is the observation of a  $180^\circ$  phase shift between the inelastic and the elastic diffraction. Nuclear physicists have called our attention to the fact that this phenomenon has been observed in  $\alpha$ -particle scattering from nuclei and has been explained by Drozdov (1955*a*, 1955*b*) and Inopin (1957) and more recently by Blair (1966). By a straightforward application of Fraunhofer diffraction theory Blair has derived the following formula for elastic scattering from a circular disc of radius  $R_0$ :

$$d\sigma/d\omega = (kR_0)^2 \{2F_1^2(\theta)/\pi x^3\} \cos^2(x + \frac{1}{4}\pi), \quad (1)$$

where  $x = kR_0\theta$  and  $F_1(\theta)$  is a form factor taking into account the 'fuzziness' of the potential. For a disc with no fuzziness we have  $F_1(\theta) = 1$ . The approximation is expected to be valid for  $x \gtrsim \frac{1}{2}\pi$ . A similar formula for inelastic scattering can be derived for a deformed hard sphere by assuming that the surface is given by  $R = R_0\{1 + \delta_2 P_2(\theta, \phi)\}$ , where  $\delta_2$  is the deformation parameter. The result in this case ( $x > \frac{1}{2}I\pi$ ) for the transition  $0 \rightarrow I$  is

$$\frac{d\sigma}{d\omega}(0 \rightarrow I) = \frac{\delta_2^2(kR_0)^2}{4\pi^2 x} 2F_1^2(\theta) \sin^2(x + \frac{1}{4}\pi), \quad I \text{ even}; \quad (2a)$$

$$= \frac{\delta_2^2(kR_0)^2}{4\pi^2 x} 2F_1^2(\theta) \cos^2(x + \frac{1}{4}\pi), \quad I \text{ odd}. \quad (2b)$$

As an aside we note that this approximation is essentially similar to a DWBA calculation. Assumptions similar to those inherent in the IOS theory are also involved. Thus the Fraunhofer model predicts that for even transitions and deformations the inelastic diffraction undulations will be shifted in phase with respect to the elastic undulations, while for odd transitions resulting from odd deformations, there will be no phase shift. Moreover, from the relative amplitudes of the elastic and inelastic scattering, M. Faubel (personal communication) in our laboratory has determined the deformation parameter. This is illustrated in Fig. 5, where the best fit is obtained for a deformation parameter of  $\delta_2 = 0.66 \text{ \AA}$ . It is gratifying to report that similar measurements for the molecule  $\text{CH}_4$  (Faubel *et al.* 1980; Kohl 1982), which has odd interaction terms and transitions, show inelastic diffraction that is in phase with the elastic diffraction, in agreement with the model.

(d) *Test of Tang-Toennies Potential Model*

Several years ago Tang and Toennies (1977) introduced a simple model for the van der Waals potential. In this model the entire potential is assumed to consist of three additive contributions:

$$V(R, \gamma) = V_{\text{SCF}}(R, \gamma) + V_{\text{disp}}(R, \gamma) + V_{\text{corr}}(R, \gamma), \quad (3)$$

where  $R$  is the internuclear distance and  $\gamma$  the angle between the molecular axis and  $R$ . Here  $V_{\text{SCF}}$  is obtained from highly accurate self-consistent field calculations for a wide range of  $R$  and for two or three different orientations  $\gamma$ ,  $V_{\text{disp}}$  is accurately estimated ( $\approx 1\%$ ) from frequency dependent polarizabilities and is corrected for the asymptotic divergence of the usual  $R^{-n}$  dispersion series, and  $V_{\text{corr}}$  is estimated from a semiclassical Drude model and takes account of the change in the dispersion potential in the well region due to the repulsive interaction. In a series of four papers Tang and Toennies (1977, 1978, 1981, 1982) have shown that this model can predict 12 atom-atom potentials and the best known anisotropic interactions for  $\text{H}_2$  with He, Ne, Ar, Kr and Xe, as well as the entire potential hypersurface for He- $\text{H}_2$  and Ne- $\text{H}_2$ . The new experiments make it possible to extend the tests of this model to more typical systems.

The potential for He- $\text{N}_2$  was calculated in collaboration with Habitz *et al.* (1982), and the results for the leading terms in the Legendre expansion,

$$V(R, \gamma) = v_0(R) + v_2(R)P_2(\cos \gamma) + v_4(R)P_4(\cos \gamma), \quad (4)$$

are shown in Fig. 6a. Also shown in Fig. 6b are the predicted potentials for both a collinear and broadside approach.

For this potential Tang and Yung (see Faubel *et al.* 1982) have carried out essentially exact close coupling calculations of the differential cross sections. Fig. 7 shows a comparison between the predicted differential cross sections and the measurements. The agreement is surprisingly good when one realizes that no adjustable potential parameters were used in the potential calculation. To obtain a feeling for the sensitivity of the cross sections to the potential shape, we have studied the effect of slight shifts of the potentials on the differential cross sections (Faubel *et al.* 1982). From these studies we estimate the errors in the isotropic and anisotropic components of the potential to be negligible with regard to its range, but that the  $v_0$  potential is probably about 20% too shallow.

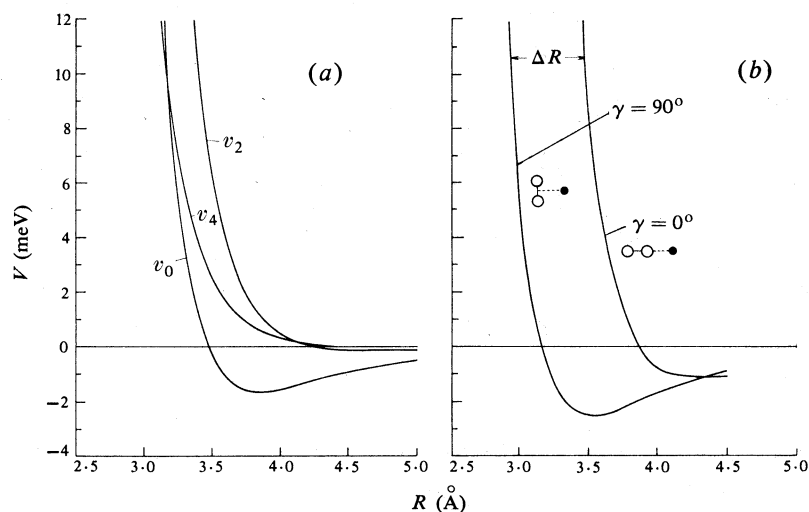


Fig. 6. Two different projections of the anisotropic potential of the form  $V(R, \gamma) = \sum_{\lambda} v_{\lambda}(R) P_{\lambda}(\cos \gamma)$  ( $\lambda$  even) for He-N<sub>2</sub> calculated using the Tang-Toennies potential model: (a) the three leading terms in the potential; (b) the potentials for both a collinear and broadside approach, where  $\Delta R = 0.55 \text{ \AA}$  ( $\delta_2 = 0.58 \text{ \AA}$ ).

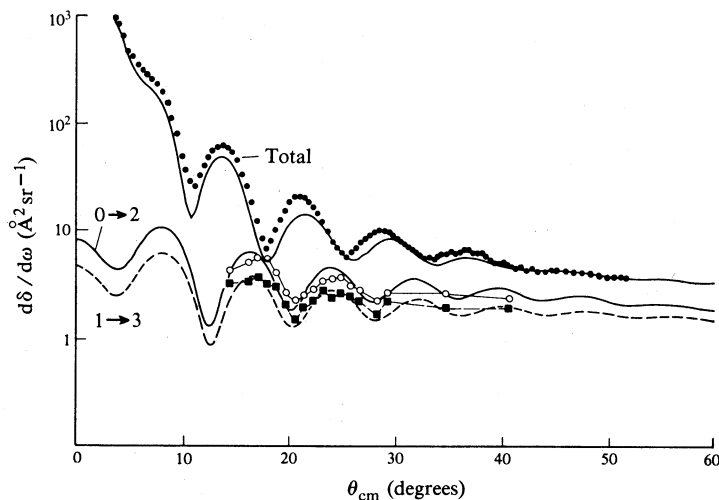


Fig. 7. Comparison of the predicted theoretical (curves) with the measured total,  $0 \rightarrow 2$  and  $1 \rightarrow 3$  differential cross sections for He-N<sub>2</sub> at  $E_{cm} = 27.3 \text{ meV}$ .

This realistic best fit potential enables us to test the deformation parameter obtained from the Fraunhofer model. From Fig. 6b we see that the Habitz-Tang-Toennies model has a deformation corresponding to  $\Delta R = 0.55 \text{ \AA}$ . It is easy to calculate  $\delta_2$  from this value and the result is  $\delta_2 = 0.58 \text{ \AA}$ , in remarkably close agreement with the Fraunhofer prediction shown in Fig. 5. Finally, the realistic potential in Fig. 6 provides a clue as to why this Fraunhofer behaviour had not been observed in previous studies of H<sub>2</sub> rotational excitation. Comparison of the anisotropic

potential curves for H<sub>2</sub> interactions similar to Fig. 6 reveals that for all the previously studied H<sub>2</sub> systems the anisotropic terms have a shorter range than the isotropic terms. This is perhaps not unexpected since it is well known that H<sub>2</sub> is a particularly spherical molecule. Moreover, the anisotropic potentials are also softer than the isotropic terms, which stems from the relatively few electrons in the outer shell. Both differences mean that the model of a deformed hard sphere no longer applies for H<sub>2</sub> interactions. Since we have seen Fraunhofer behaviour in O<sub>2</sub> and CO, and CH<sub>4</sub> as well, it thus appears to be quite a general phenomenon. Presently, we are fitting the He-O<sub>2</sub> data to a realistic potential (Kohl *et al.* 1982).

### 3. Vibrational Excitation for H<sup>+</sup> and Na<sup>+</sup> on CF<sub>4</sub>

#### (a) Apparatus

The apparatus is basically similar to that described in Section 2a. The ions are first energy selected by a 127° sector field. The monoenergetic beam is then chopped into short bursts and the flight times of the scattered ions, arriving at an open multiplier, are measured electronically. Since the flight tube is long (1.6–2 m) the ion source is rotated about the target nozzle beam in order to observe the scattering in a plane perpendicular to the nozzle beam (Rudolph and Toennies 1976).

In the H<sup>+</sup> apparatus the ions are produced in a modified Colutron source, the major modification being that all insulators have been removed and the entire discharge region is made of stainless steel. The ions are extracted through a hole 0.5 mm in diameter at 400 eV and focussed to produce a virtual object slit at the exit of a small compact 60° electromagnet of radius 5 cm. By using a large magnetic yoke and a small gap (7 mm), stray fields can be kept to a minimum. The ions are then decelerated to their final energy in a compact thick-lens ion optics and subsequently energy selected by a 127° sector field arrangement of radius 5 cm, with a relative energy resolution of  $\Delta E/E \approx 0.004$ . The remaining part of the beam passes a condenser plate pulser, which deflects the beam to one side except for short periods during which the electric potential is set equal to zero. Finally the beam is focussed onto the scattering target.

In experiments with Na<sup>+</sup> ions (Eastes *et al.* 1979), the ions are produced in a surface ionization source and then pass directly through the sector field and pulser as described above.

In both experiments the target was a skimmed molecular nozzle beam. The beam was expanded from a stagnation chamber (at a pressure of 1–2 bar or  $1\text{--}2 \times 10^2$  kPa) at room temperature through a thin walled orifice (of diameter 0.1 mm). The skimmer with cone angles of 40°/50° and opening diameter of 0.6 mm was located about 10 mm downstream from the orifice and crossed the ion beam at about 30 mm from the nozzle orifice. The population of vibrationally excited molecules in the various modes in CF<sub>4</sub> in the expanded beam is expected to be less than 10% and the most probable rotational state is  $j = 4$ . Mass spectra measurements show no evidence of dimerization.

The TOF spectra were recorded in a minicomputer using a channel width of 0.02  $\mu$ s. Typical measuring times ranged between 4 hours at small angles and up to 80 hours at large angles. Since the channel width was much less than the resolution of the machine, the spectra could be smoothed by taking a sliding average. The total count over five channels was used as the count rate for the central channel.

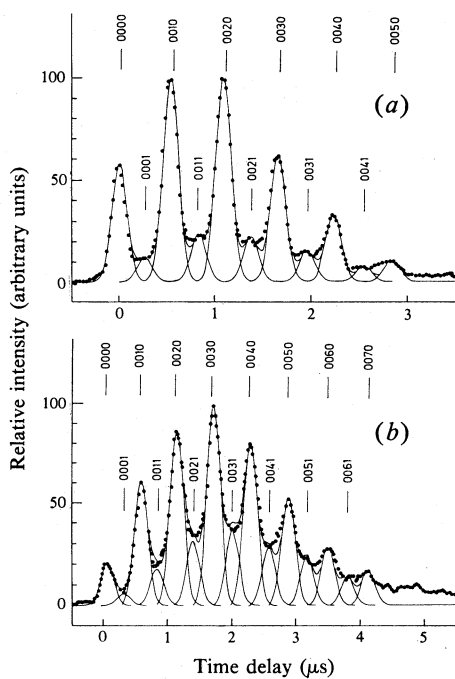


**Fig. 8.** TOF spectra measured for  $\text{H}^+-\text{CF}_4$  at  $E_{\text{lab}} = 9.8 \text{ eV}$  ( $\approx E_{\text{cm}}$ ) at (a)  $\theta_{\text{lab}} = 10.0^\circ$  and (b)  $\theta_{\text{lab}} = 15.0^\circ$ . The vertical bars indicate the vibrational quantum numbers of the different modes ( $\nu_1 \nu_2 \nu_3 \nu_4$ ) assigned to the different maxima. The small maxima between the main peaks are attributed to combination band transitions.

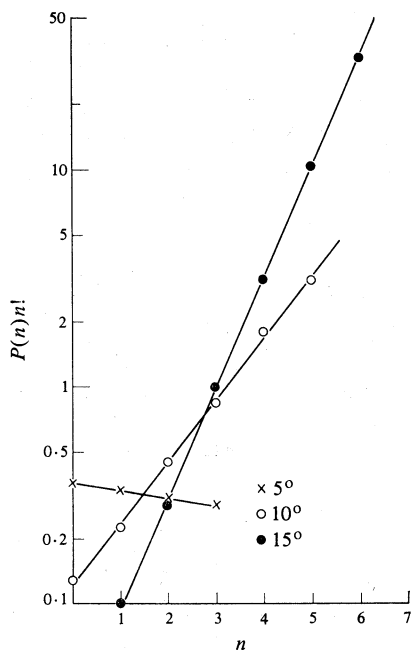


**Fig. 9.** Relative transition probabilities measured for  $\text{H}^+-\text{CF}_4$  at  $E_{\text{lab}} = 9.8 \text{ eV}$  are plotted for three scattering angles to determine if they fall on a Poisson distribution (see equation 5). From the slope of the straight line the energy transferred to the vibrational  $\nu_3$  mode is determined.

(b) TOF Spectra for  $H^+ - CF_4$

Fig. 8 shows two typical TOF spectra at  $E_{lab} = 9.8 \text{ eV}$  ( $\approx E_{cm}$ ) at  $10^\circ$  and  $15^\circ$ , which are less than the rainbow angle estimated to be at  $\theta = 36^\circ$  (Gierz *et al.* 1982b). The spectra show a clear resolution of overtone excitation of the  $\nu_3$  mode up to the seventh overtone. In addition, there is good evidence in these spectra and similar spectra for  $D^+$  for excitation of the other infrared active  $\nu_4$  mode. These secondary weakly resolved peaks correspond to combination band excitations. The resolution in these measurements is better than 50 meV (FWHM) in the scattered peaks and thus the relative energy resolution is 0.5%. Careful examination of the spectra in Fig. 8 reveals two remarkable features. First, the peak heights follow a smooth distribution, the maximum of which is shifted with increasing angle to higher levels. This shift is so extreme that little flux is left over for the elastic transition, especially in the  $15^\circ$  measurement (Fig. 8b). Secondly, the  $\nu_3$  peaks all lie within less than 9 meV of the location for the rotationally elastic peak. Note also that the peak locations can be determined to a precision of better than 5 meV. Thus there is no evidence for any rotationally inelastic excitation within these limits (Ellenbroek and Toennies 1982).

To determine if the relative probabilities follow a Poisson distribution

$$P(0 \rightarrow n) = (1/n!) \exp(-\varepsilon) \varepsilon^n, \quad (5)$$

where  $\varepsilon = \Delta E/\hbar\omega$  and  $\Delta E$  is the first moment of the energy transfer distribution, we have plotted the measured ratios  $\ln P(n)/n!$  against  $n$  in Fig. 9. If the assumption of a Poisson distribution is correct, then all the points at one scattering angle should fall on a straight line, the slope of which provides a direct measure of  $\varepsilon$ . Fig. 9 reveals that all the points up to the highest  $n$  do in fact lie on a Poisson distribution. This remarkable result suggests that mode-to-mode coupling is not occurring in the course of these collisions (where collision times are  $\approx 10^{-14}$  s) and, furthermore, that we can model the interaction by assuming a simple forced oscillation interaction

$$m\ddot{Q} + kQ = F(t), \quad (6)$$

where  $Q$  is a normal mode coordinate, transformed along the direction of  $R$  at closest approach,  $k$  is the spring constant and  $F(t)$  is the time-dependent force. The predominant coupling to the  $\nu_3$  mode comes from the charge-induced dipole interaction (Jackson 1962; Ellenbroek *et al.* 1980)

$$V(Q, t) = (d\mu/dQ)Q \mathcal{E}(t), \quad (7)$$

where  $\mathcal{E}(t)$  is the time-dependent electric field experienced by the molecule. The energy transfer to a forced oscillator is given by (Ellenbroek *et al.* 1980)

$$\Delta E = (2\pi/m) |d\mu/dQ|^2 |\mathcal{E}(\omega)|^2, \quad (8)$$

where  $\mathcal{E}(\omega)$  is the Fourier component of the field at frequency  $\omega$  of the excited mode,

$$\mathcal{E}(\omega) = \frac{1}{(2\pi)^{\frac{1}{2}}} \int_{-\infty}^{+\infty} \mathcal{E}(t) \exp(-i\omega t) dt, \quad (9)$$

where the integral is over the trajectory. Thus the predominantly excited mode depends on which mode has the greatest value of  $\mathcal{E}(\omega)$ .

Calculations by Ellenbroek and Toennies (1982) reveal very good agreement between experimental  $\Delta E$  values and predicted values based on extensive classical calculations, which are essentially a refinement of this simple model. This is rather surprising when one realizes that the field strengths are of the order of  $10^8 \text{ V cm}^{-1}$  and consequently greater than those achieved in the most powerful Q-switched lasers. Thus we can consider the use of  $\Delta E$  measured in these scattering experiments to determine  $|d\mu/dQ|$ . Since the experiment requires no absolute calibration, this method may be more precise than the standard one involving a measurement of absolute infrared line strengths. Also, with some improvement in energy resolution, it should be possible to obtain direct spectroscopic information on the energy levels of high lying vibrational states, which is not presently possible using infrared spectroscopy. Noll (1982) in our laboratory has found a predominance of single-mode excitation in similar scattering experiments on the following fluorinated hydrocarbons:  $\text{CH}_3\text{F}$ ,  $\text{CF}_3\text{H}$ ,  $\text{C}_2\text{H}_3\text{F}$ ,  $\text{C}_2\text{H}_2\text{F}_2$ ,  $\text{C}_2\text{F}_3\text{H}$ ,  $\text{C}_2\text{F}_4$  and  $\text{C}_2\text{F}_6$ . For pure hydrocarbons the excitation of a single mode is not so pronounced, in accord with the observed and largely understood (Ellenbroek and Toennies 1982) differences between  $\text{CF}_4$  and  $\text{CH}_4$  in scattering with  $\text{H}^+$  and  $\text{Li}^+$ .

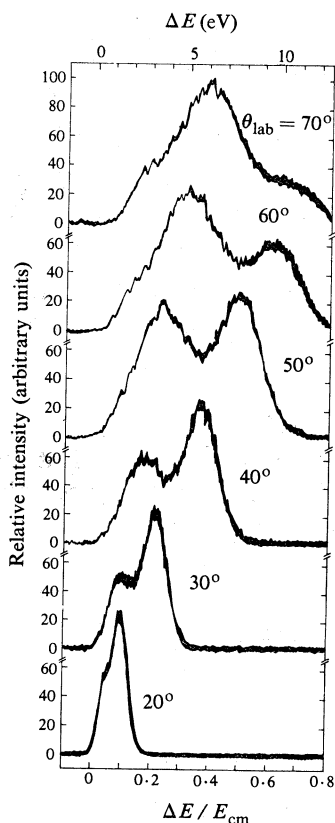


**Fig. 10.** TOF spectra measured for  $\text{Na}^+ - \text{CF}_4$  at  $E_{\text{lab}} = 19.8 \text{ eV}$  ( $E_{\text{cm}} = 15.7 \text{ eV}$ ) at low TOF resolution, but at large angles. The second peak at large energy transfers is attributed to a direct interaction with the F atoms in the molecule.

(c) *TOF Spectra for  $\text{Na}^+ - \text{CF}_4$*

Until recently we had only been able to study these excitation processes up to scattering angles of about  $20^\circ - 30^\circ$ . In order to go to larger angles, Gierz and Wilde

in our laboratory have modified the apparatus to increase its sensitivity by reducing its resolving power. Fig. 10 shows a series of spectra taken after this modification for  $\text{Na}^+-\text{CF}_4$  at 20 eV out to angles of  $\theta_{\text{lab}} = 70^\circ$  (Gierz *et al.* 1982c). At  $\theta = 20^\circ$  we see a behaviour reminiscent of that observed in  $\text{H}^+-\text{CF}_4$  and  $\text{Li}^+-\text{CF}_4$ . However, at larger angles a second peak appears corresponding to roughly twice the energy transfer.

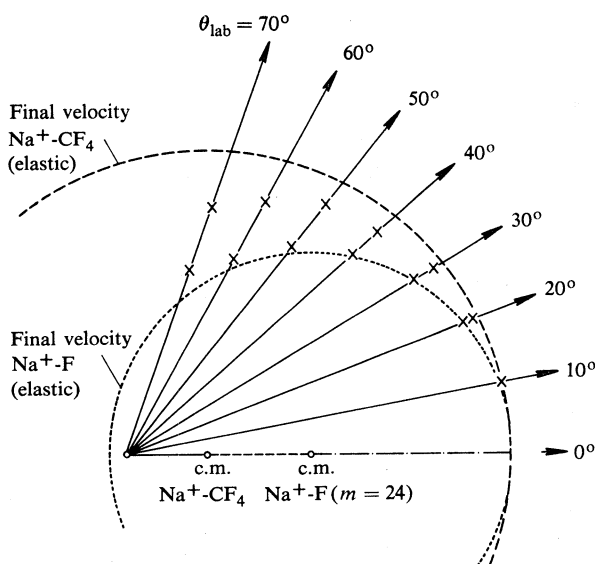


**Fig. 11.** Simple Newton velocity diagram used to identify the mechanisms responsible for the two energy-loss peaks in Fig. 10. If we assume the  $\text{CF}_4$  to be stationary, the incident lab velocity of  $\text{Na}^+$  is divided into two parts: the c.m. velocity of the entire  $\text{Na}^+-\text{CF}_4$  system and the velocity of  $\text{Na}^+$  in the c.m. system. The final scattering velocities for elastic scattering are expected to lie on the dashed circle. The dotted circle indicates the final velocities for scattering from one of the F atoms (with effective mass 24 a.m.u.) in the molecule.

To explain this second peak, we show in Fig. 11 a Newton velocity diagram, which is greatly simplified by neglecting the velocity of the  $\text{CF}_4$  molecule relative to that of  $\text{Na}^+$ . The crosses show the locations of both maxima. The dashed circle shows the velocities of events, corresponding to elastic scattering from the molecule. The fast peaks thus appear to be due to inelastic scattering from the molecule, as described in the previous subsection. The second peak, measured at different lab angles, is found to fall on a common circle, centred around a different point. From the measurements we find that this central point corresponds to a c.m. velocity in which the target particle has a mass of 24 a.m.u. From this observation we infer that the second peak can be attributed to elastic scattering from the F atoms ( $m = 19$  a.m.u.). Thus the F atoms behave as free targets, even though they are actually tightly bonded to the C atoms (with a bond dissociation energy of  $\approx 5.6$  eV). We have several descriptive names for this effect: punching bag effect; Compton effect in molecules; spectator or impulsive scattering from constituents. In itself this phenomenon is neither surprising nor new in that it has been observed previously

**Table 1.** Collision partners studied at collision energies between 5–30 eV and at large scattering angles  $\theta > 30^\circ$

A plus indicates the presence of a second peak, suggesting impulsive scattering from a constituent of the molecule, and a minus indicates no evidence for impulsive scattering

Ion	O <sub>2</sub>	N <sub>2</sub>	CO <sub>2</sub>	N <sub>2</sub> O	CH <sub>4</sub>	CF <sub>4</sub>	CHF <sub>3</sub>	CCl <sub>4</sub>	SF <sub>6</sub>	C <sub>2</sub> H <sub>6</sub>
Li <sup>+</sup>		+	-			+				
Na <sup>+</sup>	+?	+?	-	-	-	+	+		+	-?
K <sup>+</sup>	-					+		+	+	

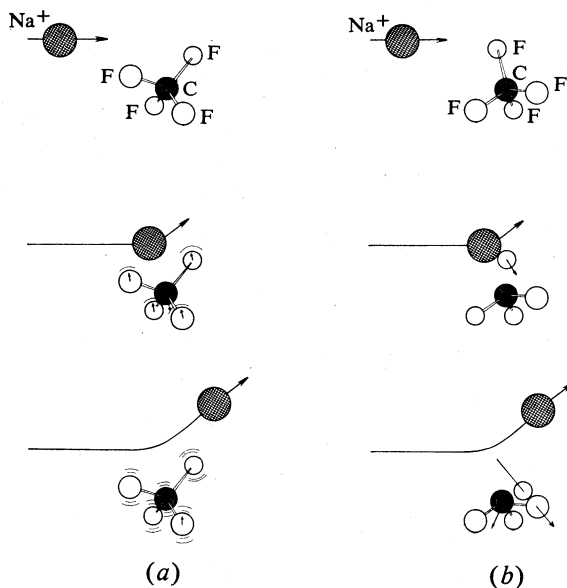


**Fig. 12.** Simplified billiard-ball model of the two collision mechanisms found to occur for fast ions with a large number of molecules, illustrated for the collision  $\text{Na}^+ - \text{CF}_4$ . The atomic and ionic radii are drawn to scale, but are reduced for clarity by a factor of two compared with the bond distances. We show (a) the normal mode excitation of the  $\nu_3$  mode, involving a collective excitation of the entire molecule, and (b) the local excitation, where the ion interacts only with a single essentially free F atom.

at keV energies (Sigmund 1978) and also for  $\text{Li}^+ - \text{H}_2$  dissociation down to about 50–60 eV (Schöttler and Toennies 1974). However, in all the previous examples electronically inelastic processes could also occur. What is remarkable here is that we have been able to trace this double-peak behaviour down to energies of  $E_{\text{cm}} \approx 5$  eV, corresponding to an  $\text{Na}^+ - \text{F}$  energy of only 2.5 eV.\* At these energies the collisions are expected to be electronically adiabatic (the energy of the first electronically excited level is estimated to be about 9 eV). Thus, as a result of these new experiments we are forced to revise our previous ideas about single centre

\* The spectra at 5 eV are not nearly as nice as those in Fig. 10 at 15.7 eV because of much greater noise at the lower intensities and because of smearing, since the target velocity spread makes a significant contribution.

expansions of the adiabatic potentials between ions (or atoms) and polyatomic molecules at these energies to include the direct interaction with the constituent atoms.

We have looked for this direct interaction effect in the partner combinations listed in Table 1, where a plus indicates that we have seen an impulsive peak and a minus indicates that we did not see the effect. So far we have no explanation for the fact that some systems show this phenomenon and some do not.

Finally we summarize this section with a simple picture. Fig. 12 illustrates the two different collision mechanisms which we have found for fast ions on polyatomic molecules. We expect this new effect to also occur for neutral particle systems, where it may play a very important role in vibrational excitation and dissociation.

#### 4. Discussion

In the work presented here we have demonstrated that at least under certain conditions relatively simple models may be quite useful in predicting interaction potentials. The He-N<sub>2</sub> experiments show for the first time that the Tang-Toennies (1977, 1978, 1981, 1982) model is capable of providing a very good prediction of the potentials involving heavy diatomics such as N<sub>2</sub>. The model can now be easily extended to treat systems such as Ne-N<sub>2</sub> and Ar-N<sub>2</sub>, and Habitz is presently carrying out the required SCF calculations. The next step will be to tackle the N<sub>2</sub>-N<sub>2</sub> system using the model, for which it will still take some time to be able to do the beam experiments with sufficient state resolution. Of course, we hope to test the potential model further by applying it to He-O<sub>2</sub> and He-CO where, however, our knowledge of the dispersion coefficients is not really satisfactory enough to make firm predictions. The Fraunhofer model indicates that the data can be 'inverted' in a simple way to obtain the repulsive anisotropy. Perhaps with some modifications it will be possible to increase the accuracy of the Fraunhofer model and to also determine anisotropies for the different Legendre terms in the potential and even the shape of these terms.

The extensive studies of vibrational excitation of polyatomic molecules using ions has reinstated the old forced oscillator model as a valid model for vibrational excitation. Apparently the model works well so long as the interaction does not deviate too far from a linear force law and provided that rotational excitation and mode-to-mode coupling do not occur during the course of the collision. Also, the experiments indicate that the basic idea of a breathing sphere model with neglect of rotations may also be a valid approximation, at least at sufficiently high collision energies ( $E_{cm} \gtrsim 5$  eV). The present evidence based on comparisons with theoretical calculations indicates that the inelastic cross sections can be used to determine infrared and other vibrational coupling constants of a large number of molecules. Conversely, since we know the interaction laws, we hope to eventually probe mode-to-mode dynamics by looking for deviations from the Poisson distribution. The evidence in this direction has however been meagre so far.

The impulsive collision mechanism found recently is intriguing since it shows a new mechanism for efficient vibrational excitation of diatomic and polyatomic molecules. This mechanism has been anticipated in previous theoretical studies of energy transfer (Villalonga *et al.* 1979; Micha 1981). In future experiments we hope to learn more about this process by determining the effective mass of the

atomic targets more precisely and to increase the resolution to determine the natural line broadening of the peaks, and from this the velocity distribution of the atoms in the molecule.

### Acknowledgments

I am grateful to M. Faubel and K. H. Kohl for permission to present here some results on the Fraunhofer model, not published previously. Also I am grateful to M. Noll, U. Gierz and M. Wilde for their consent to my presenting their previously unpublished results on  $H^+-CF_4$  and  $Na^+-CF_4$ . I thank all of the above for their active collaboration.

### References

- Bergmann, K., Engelhardt, R., Hefter, U., Hering, P., and Witt, J. (1979). *J. Chem. Phys.* **71**, 2726.
- Bergmann, K., Hefter, U., Mattheus, A., and Witt, J. (1981). *Chem. Phys. Lett.* **78**, 61.
- Bischof, G., Hermann, V., Krutein, K., and Linder, F. (1982). *J. Phys. B* **15**, 249.
- Blair, J. S. (1966). In 'Lectures in Theoretical Physics', Vol. VIII C, p. 343 ff. (Univ. Colorado Press: Boulder).
- Brusdeylins, G., Meyer, H.-D., Toennies, J. P., and Winkelmann, K. (1977). *Prog. Astronaut. Aeronaut.* **51**, 1047.
- Buck, U., Huisken, F., and Schleusener, J. (1978). *J. Chem. Phys.* **68**, 5654.
- Buck, U., Huisken, F., Schleusener, J., and Schaefer, J. (1981). *J. Chem. Phys.* **74**, 535.
- Drozdov, S. I. (1955a). *Sov. Phys. JETP* **1**, 788.
- Drozdov, S. I. (1955b). *Sov. Phys. JETP* **1**, 791.
- Eastes, W., Ross, U., and Toennies, J. P. (1979). *J. Chem. Phys.* **70**, 1652.
- Eccles, J., Pfeffer, G., Piper, E., Ringer, G., and Toennies, J. P. (1982). (to be published).
- Ellenbroek, T., Gierz, U., Noll, M., and Toennies, J. P. (1982). *J. Phys. Chem.* **86**, 1153.
- Ellenbroek, T., Gierz, U., and Toennies, J. P. (1980). *Chem. Phys. Lett.* **70**, 459.
- Ellenbroek, T., and Toennies, J. P. (1982). *Chem. Phys.* (to be published).
- Faubel, M., Kohl, K. H., and Toennies, J. P. (1980). *J. Chem. Phys.* **73**, 2506.
- Faubel, M., Kohl, K. H., Toennies, J. P., Tang, K. T., and Yung, Y. Y. (1982). *Faraday Discuss. Chem. Soc.* **73**, 000.
- Faubel, M., and Toennies, J. P. (1977). *Adv. Atom. Mol. Phys.* **13**, 262.
- Faubel, M., and Toennies, J. P. (1979). *J. Chem. Phys.* **71**, 3770.
- Faubel, M., and Weiner, E. R. (1981). *J. Chem. Phys.* **75**, 641.
- Gentry, W. R., and Giese, C. F. (1977). *J. Chem. Phys.* **67**, 5389.
- Gianturco, F., Gierz, U., and Toennies, J. P. (1980). *J. Phys. B* **14**, 667.
- Gierz, U., Noll, M., and Toennies, J. P. (1982a). (in preparation).
- Gierz, U., Noll, M., and Toennies, J. P. (1982b). (in preparation).
- Gierz, U., Toennies, J. P., and Wilde, M. (1982c). (to be published).
- Goldflam, R., Kouri, D. R., and Green, S. (1977). *J. Chem. Phys.* **67**, 5661.
- Habitz, P., Tang, K. T., and Toennies, J. P. (1982). *Chem. Phys. Lett.* **85**, 461.
- Inopin, E. V. (1957). *Sov. Phys. JETP* **4**, 764.
- Jackson, J. D. (1962). 'Classical Electrodynamics', p. 435 (Wiley: New York).
- Kohl, K. H. (1982). Dissertation, University of Göttingen.
- Kohl, K. H., Faubel, M., Gianturco, F., and Toennies, J. P. (1982). *J. Chem. Phys.* (submitted).
- Krutein, J., and Linder, F. (1977). *J. Phys. B* **10**, 1363.
- Meyer, G., and Toennies, J. P. (1981). *J. Chem. Phys.* **75**, 2753.
- Meyer, G., and Toennies, J. P. (1982). *J. Chem. Phys.* **77**, 798.
- Micha, D. A. (1981). In 'Potential Energy Surfaces and Dynamics Calculations' (Ed. D. Truhlar), p. 703ff (Plenum: New York).
- Noll, M. (1982). Max-Planck-Institut für Strömungsforschung, Göttingen, Bericht.
- Ross, U., Schepper, W., and Beck, D. (1981). *Chem. Phys.* **61**, 95.
- Rudolph, K., and Toennies, J. P. (1976). *J. Chem. Phys.* **65**, 4483.

- Schmidt, H., Hermann, V., and Linder, F. (1976). *Chem. Phys. Lett.* **41**, 365.
- Schöttler, J., and Toennies, J. P. (1974). *Chem. Phys.* **4**, 24.
- Sigmund, P. (1978). *J. Phys. B* **11**, L145.
- Tang, K. T., and Toennies, J. P. (1977). *J. Chem. Phys.* **66**, 1496 (for errata see *ibid* (1977), **67**, 375; (1978), **68**, 786).
- Tang, K. T., and Toennies, J. P. (1978). *J. Chem. Phys.* **68**, 5501.
- Tang, K. T., and Toennies, J. P. (1981). *J. Chem. Phys.* **74**, 1148.
- Tang, K. T., and Toennies, J. P. (1982). *J. Chem. Phys.* **76**, 2524.
- Toennies, J. P. (1976). *Annu. Rev. Phys. Chem.* **27**, 225.
- Toennies, J. P., and Winkelmann, K. (1977). *J. Chem. Phys.* **66**, 3965.
- Villalonga, E., Micha, D. A., and Toennies, J. P. (1979). *Chem. Phys. Lett.* **68**, 352.

Manuscript received 6 May, accepted 6 September 1982

